Static and Dynamic Solution Properties of Corn Amylose in *N*,*N*-Dimethylacetamide with 3% LiCl

X. Cao,[†] D. J. Sessa,[‡] W. J. Wolf,[‡,§] and J. L. Willett[‡,*]

Department of Chemistry, Bradley University, Peoria, Illinois 61625; and Plant Polymer Research, USDA,[||] ARS, MWA, National Center for Agricultural Utilization Research, 1815 North University Street, Peoria, Illinois 61604

Received October 28, 1999; Revised Manuscript Received February 15, 2000

ABSTRACT: Static and dynamic light scattering techniques were used to study the solution properties of corn amylose in *N*,*N*-dimethylacetamide with 3% (w/v) LiCl. Static properties show three distinguishable regions, which are designated as the dilute, the semidilute, and the concentrated regimes. The concentrations at which these transitions occur are designated as the overlap concentration c^* and the semidilute−concentrated transition concentration c^{**}. Two master curves are used successfully to fit the static data in the dilute and semidilute regimes. Dynamic data show that at $c < c^*$, a single diffusion motion representing the translational diffusion of the amylose macromolecule is present in the solution. At $c > c^*$, two dynamic motions are observed: a fast diffusion representing the cooperative diffusion and a slow one representing the cluster diffusion. The slow diffusion motion is found to follow the "stretched exponential" diffusion law. The fast diffusion motion is found to have two distinguishable concentration dependence patterns: its concentration dependence at $c > c^{**}$ is stronger than that at $c < c^{**}$. The relative amounts of these two modes are also analyzed in terms of their concentration dependence.

Introduction

Starch is the major form of carbohydrate storage in green plants and is the second largest biomass produced on earth. Starch polymer is a mixture of two macromolecular α-glucans: the essentially linear amylose and the highly branched amylopectin. Depending on botanical origin and genetic background, different starches have different chemical structures, such as amylose contents and branch-chain length. This structural and functional diversity makes these starches suitable for different applications, ranging from the food industry to biomedical applications. Starch is also a renewable resource which has significant cost advantage over commercial synthetic polymers. This cost advantage, along with biodegradability properties, has led to starch being used in conjunction with synthetic polymers to produce blends and composites. Many of these applications involve starch dispersion and solution. The solution properties of starch are greatly influenced by starch's structural characteristics, such as molecular dimensions, and hydrodynamic behavior.

Static and dynamic light scattering measurements have been used successfully to study starch's molecular characteristics as well as starch's solution properties.[1−11] However, many of these studies used various native starches as solute, and the coexistence of amylose and amylopectin made the data interpretation rather complicated and difficult. Moreover, most of the reported studies have been conducted in either aqueous or DMSO/H_2O solutions. Aqueous solutions are notorious for generating dust problems in light scattering experiments because of water's high affinity to dust particles. In addition, dissolution of starch in aqueous solvents can result in erroneously high molecular weight due to incomplete dissolution; also, extreme sample treatments such as autoclaving and high pH, which are often required to dissolve starch in H_2O, can result in molecular size reduction due to degradation and oxidation.

N,*N*-dimethylacetamide with 3% (w/v) LiCl (DMAc−3% LiCl) solvent mixture has been used to solubilize cellulose[12] as well as wormlike aromatic polyamide polymers such as poly(1,4-benzamide).[13] Our study shows that the DMAc−3% LiCl solvent can also be used to dissolve starch. The present work reports our recent experimental results on static and dynamic solution properties of purified corn amylose in DMAc−3% LiCl.

Experimental Section

Chemicals. Purified corn amylose was kindly provided by Dr. C. Knutson of USDA, ARS, MWA, National Center for Agricultural Utilization Research, Peoria, IL. The corn amylose was purified by 3−5 crystallizations from butanol according to Schoch.[14] The purity of the corn amylose sample was checked by the amylose-iodine complex method, and it was determined that this corn amylose was the purest available.[15] The solvent mixture was prepared by dissolving 3% LiCl (99+%, ACS reagent grade, Aldrich, Milwaukee, WI) in DMAc (HPLC grade, 99.9%, Aldrich).

Solution Preparations. Amylose solutions of concentrations higher than 2.0 mg/mL were prepared by mixing the appropriate amounts of amylose with 8 mL of DMAc−3% LiCl solvent in 10 mL Reacti-Vials (Pierce, Rockford, IL). The mixtures were allowed to stand at room temperature for 2 h and then gradually heated to 80 °C in 3 h under gentle stirring. The mixtures were then heated to 120 °C in 1 h and then maintained at 120° for 5 min. The vial caps were then tightened, and the mixtures were air-cooled to room temperature. Solutions with concentrations lower than 2.0 mg/mL were prepared by dilution from a stock solution of 3.0 mg/mL prepared by the above method.

Solutions for light scattering (LS) experiments were filtered through Whatman (Clifton, NJ) disposable syringe filters

[†] Bradley University.
[‡] National Center for Agricultural Utilization Research.
[§] Retired.
[||] "Names are necessary to report factually on available data; however, the USDA neither guarantees nor warrants the standard of the product, and the use of the name by USDA implies no approval of the product to the exclusion of others that may also be suitable."

10.1021/ma9918248 CCC: $19.00
Published on Web 04/13/2000

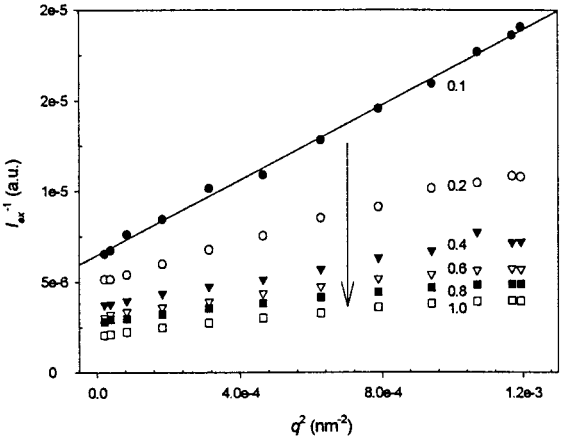

Figure 1. Scattering intensity of corn amylose in DMAc−3% LiCl, measured at 25.0 °C. $I_{ex} = I_{solution} - I_{solvent}$. The straight line shows the linear least-squares fit, and from its slope, R_G was calculated according to eq 1 (Zimm plot method). The arrow shows the direction of increases in the solution concentration c. Note that the scattering intensity increases as c increases. For clarity, only 6 out of 19 sets of data are shown. Concentrations in milligrams per milliliter are indicated.

(PTFE filter media with polypropylene housing, 25 mm diameter, 0.2 μm pore size), into acetone-rinsed and dried scintillation vials (SV) for measurement. Nineteen concentrations were prepared and studied, with concentrations ranging from 0.1 to 150.0 mg/mL. Solutions with concentrations higher than 150 mg/mL became un-filterable and thus unsuitable for LS studies.

Methods of Measurement. The refractive index, n, of the DMAc−3% LiCl solvent mixture was taken as $n = 1.449$ at $\lambda = 514.5$ nm, and the viscosity, η, of the solvent mixture was taken as $\eta = 1.354$ cP. The solvent was also reported to have no absorption peak in the wavelength range between 400 and 600 nm.[13]

The LS apparatus has been described elsewhere.[16] All measurements were performed with a Brookhaven Instruments Corporation (BIC, Holtsville, NY) BI-9000AT autocorrelator and a variable-scattering-angle BIC BI-200SM goniometer with a stepping motor controller. A Lexel 95 argon ion laser of $\lambda = 514.5$ nm was used as the light source, operating at 10^1-10^2 mW according to the particular measurement. All light scattering measurements were made at 25.0 °C.

Intensity measurements were collected at every 15° between 15° and 150°, plus two additional angles at 20° and 155°, for a total of 12 scattering angles, θ. Correlation functions were collected at every 15° between 30° and 150° for a total of nine scattering angles. The light scattering apparatus was calibrated by using toluene, molecular weight standard polystyrene in toluene, and polystyrene nanospheres suspended in water.

Data Analysis. *Static Data.* The following common plots were used to analyze the static light scattering (SLS) data. The first plot was the partial Zimm plot according to the following formula:

$$(I_{ex(q)})^{-1} = C_1[1 + (R_G{}^2q^2/3)] \quad (1)$$

I_{ex} is the excess intensity of scattered light, C_1 is a constant (the subsequent C_2-C_4 in eqs 2−4 are similar constants as well), R_G is the radius of gyration, and q is the scattering vector: $q = 4\pi n/\lambda \sin(\theta/2)$. Here, R_G is determined from the slope and the intercept of the plot of $(I_{ex(q)})^{-1}$ versus q^2.

The second plot was the partial Berry plot according to the following formula:

$$(1/I_{ex(q)})^{1/2} = C_2(1 + R_G{}^2q^2/6) \quad (2)$$

Here, R_G is determined from the slope and the intercept of the plot of $(1/I_{ex(q)})^{1/2}$ versus q^2.

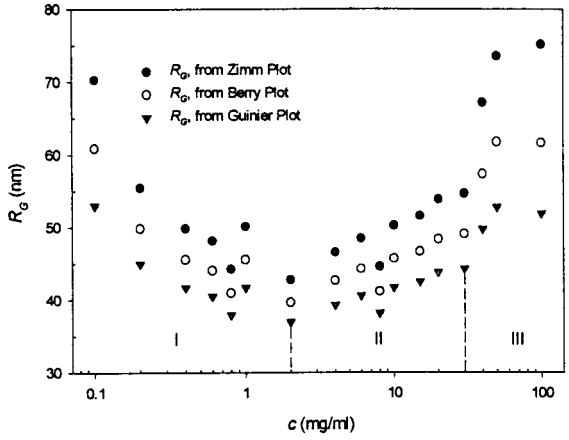

Figure 2. R_G Values of amylose at different concentration, obtained by analyzing SLS data as partially presented in Figure 1, using Zimm, Berry and Guinier methods, respectively (eqs 1, 2, and 3). Three distinguishable regions are apparent, according to the R_G's dependence on c.

The third plot was the Guinier plot:

$$I_{ex(q)} = C_3 \exp(-R_G{}^2q^2/3) \quad (3)$$

When a Guinier plot is appropriate, plotting $\ln(I_{ex(q)})^{-1}$ versus q^2 yields a straight line, and from the slope, R_G is determined.

The fourth plot was the fractal plot:

$$I_{ex(q)} = C_4q^{-d_f} \quad (4)$$

When a fractal plot is appropriate, plotting $\ln(I_{ex(q)})$ versus $\ln(q)$ yields a straight line, and the fractal dimension d_f is thus obtained as the slope.

Data Analysis. *Dynamic Data.* The analysis of measured correlation function $G_2(t)$, by dynamic light scattering (DLS), has been described elsewhere.[16] In brief, the distribution $A(D)$ of species with diffusion coefficient D from the normalized electric field autocorrelation function $g_1(t)$, which was calculated from $G_2(t)$, was obtained by using the regularized positive exponential sum (REPES) program, which employs the Laplace inversion.[17−20]

$$g_1(t) = \int A(D) \exp(-Dq^2t)\, dD \quad (5)$$

Results and Discussion

Static Properties. Figure 1 shows the plot of the reciprocal scattering intensity against q^2 for the 19 concentrations of corn amylose in DMAc−3% LiCl. Equations 1−4 were used to fit the experimental data. To be consistent, all measured data points were included in the fitting, and the fitting results are summarized in Table 1. The least-squares fitting gives an R_G with a standard deviation. In addition, it also gives the reduced χ^2, which is a relative measure of the goodness of the fit. Two features of the results are evident, as shown in Table 1: (1) the reduced χ^2 increases as the concentration increases regardless of the equations used, indicating that the goodness of the fitting deteriorates; and (2) at concentration $c \leq 30.0$ mg/mL, the Zimm plot gives the best fit (smallest reduced χ^2), whereas at concentrations $c \geq 40.0$ mg/mL, the fractal plot gives the best fit in general.

Figure 2 shows the R_G values for amylose in DMAc−3% LiCl as a function of amylose concentration, obtained from SLS data via different fitting methods. Analyzing the same set of SLS data using the three calculation methods, namely, the Zimm, Berry, and Guinier plots,

Table 1. Static Parameters of Amylose in DMAc−3% LiCl Measured by Static Light Scattering at 25.0 °C

sample	c (mg/mL)	Zimm R_G (nm)	reduced χ^2	Berry R_G (nm)	reduced χ^2	Guinier R_G (nm)	reduced χ^2	fractal d_f	reduced χ^2
1	0.1	70.3 ± 0.086	37.8	60.9 ± 0.049	93.4	53.0 ± 0.089	213	0.46 ± 0.002	800
2	0.2	55.5 ± 0.062	23.5	49.9 ± 0.038	69.1	45.0 ± 0.077	150	0.35 ± 0.001	915
3	0.4	49.9 ± 0.053	30.5	45.6 ± 0.033	77.3	41.7 ± 0.073	153	0.30 ± 0.001	930
4	0.6	48.2 ± 0.045	144	44.1 ± 0.029	224	40.5 ± 0.063	328	0.30 ± 0.001	641
5	0.8	44.3 ± 0.043	120	41.0 ± 0.028	184	38.0 ± 0.063	264	0.27 ± 0.001	647
6	1.0	50.2 ± 0.041	198	45.6 ± 0.026	335	41.7 ± 0.055	513	0.32 ± 0.001	846
7	2.0	42.8 ± 0.036	259	39.7 ± 0.024	359	37.0 ± 0.055	484	0.26 ± 0.001	871
8	4.0	46.6 ± 0.034	518	42.7 ± 0.022	722	39.3 ± 0.048	964	0.30 ± 0.001	649
9	6.0	48.5 ± 0.033	447	44.3 ± 0.022	674	40.6 ± 0.046	956	0.31 ± 0.001	1020
10	8.0	44.6 ± 0.034	295	41.2 ± 0.023	431	38.2 ± 0.050	599	0.27 ± 0.001	1010
11	10.0	50.3 ± 0.034	623	45.7 ± 0.022	914	41.7 ± 0.045	1280	0.33 ± 0.001	1050
12	15.0	51.6 ± 0.034	383	46.7 ± 0.022	630	42.5 ± 0.043	955	0.33 ± 0.001	1690
13	20.0	53.9 ± 0.034	433	48.4 ± 0.022	734	43.8 ± 0.042	1130	0.36 ± 0.001	1430
14	30.0	54.7 ± 0.034	298	49.1 ± 0.021	577	44.3 ± 0.042	965	0.36 ± 0.001	2000
15	40.0	67.2 ± 0.051	1820	57.4 ± 0.031	2340	49.8 ± 0.056	2900	0.48 ± 0.001	287
16	50.0	73.6 ± 0.054	1730	61.8 ± 0.031	2430	52.8 ± 0.054	3280	0.53 ± 0.000	285
17	75.0	197.4 ± 0.1	11500	118.6 ± 0.03	25800	81.5 ± 0.034	51300	1.27 ± 0.001	5110
18	100.0	75.2 ± 0.046	7540	61.7 ± 0.027	936	51.9 ± 0.049	11000	0.55 ± 0.001	2500
19	150.0	299.5 ± 0.6	8470	144.2 ± 0.07	17400	89.3 ± 0.07	33200	1.60 ± 0.002	9470

gives different R_G values for the polymer. However, for R_G as a function of amylose concentration, the three methods give similar trends. The whole concentration range of the measurements, $c = 0.1-150$ mg/mL, can be divided into three regions according to the R_G's dependence on c. Region I is in the range of $0.1 \le c \le \sim 2$ mg/mL, where R_G monotonically decreases with increasing c. Region II is in the range of $\sim 2 \le c \le \sim 30$ mg/mL, where R_G monotonically increases with increasing c. Region III is at $c \ge \sim 30$ mg/mL, where, as in region II, R_G increases with increasing c, but at a much higher rate.

The monotonic decrease of R_G with increasing c (region I) can be explained by the following relationship for polymers in dilute concentration regime:

$$1/R = 1/R_0\,(1 + kc) \tag{6}$$

where R_0 is the radius of the polymer at infinite dilution and k is a constant. The increase of R_G in region II is probably due to the fact that the concentration in this region is high enough that the amylose macromolecules start to overlap and to form aggregates. In other words, region II is the semidilute region, and the concentration $c \sim 2$ mg/mL is the so-called overlap concentration c^*. Region III is, by logic, the concentrated region.

The value for c^* can be theoretically calculated, according to the following relationship,[21]

$$c_{R_G}{}^* = \frac{M_W/N_A}{\frac{4\pi}{3}R_G{}^3} \tag{7}$$

By use of eq 6 and the R_G values from Zimm plots in the concentration range of 0.1−1.0 mg/mL, an $R_G = 63.1$ nm at $c = 0$ is then obtained. M_W values for corn amylose have been reported to range from $M_W \sim 5.0 \times 10^5$ g/mol[22] to 2.0×10^6 g/mol.[1] Combining these M_W values and $R_G = 63.1$ nm, eq 7 gives $c_{R_G}{}^*$ values ranging from $c_{R_G}{}^* \sim 0.8$ to $c_{R_G}{}^* \sim 3$ mg/mL. Therefore, the observed c^* value ($c^* \sim 2$ mg/mL, as discussed above), is in agreement with the estimated $c_{R_G}{}^*$ values.

The concentration at which the solution undergoes the transition from semidilute regime to concentrated regime is designated as c^{**}. It has been proposed that c^{**} can be crudely approximated as $c^{**} \sim (^{10}/_3)c^*$.[23−26] According to this approximation, a value of $c^{**} \sim 7$ mg/mL is obtained for our amylose in a DMAc−3% LiCl system. This value is far below the concentration, ~30 mg/mL, at which the transition from region II to region III is observed to occur. However, an equation for c^{**} for wormlike macromolecules has been recently proposed,[13]

$$c^{**} = \frac{0.243M/N_A}{(L/L_p)^{1/4}dL_pL} \tag{8}$$

where L is the contour length, d is the diameter, and L_P is the persistence length. By use of $R_G = 63.1$ nm, combined with other macromolecular parameters reported in the literature,[8] a persistence length of $L_P = 3.26$ nm is then calculated for amylose in DMAc−3% LiCl by following the procedure of Hanemann and Ballauff for cellulose in a solution of $Cu(OH)_2$ in aqueous ammonia.[27] Through the insertion of $L_P = 3.26$ nm, $d = 1.32$ nm,[28] and other molecular parameters of amylose into eq 8, a c^{**} range of 7−11 mg/mL is then obtained.

These estimated c^{**} values, i.e., $c^{**} \sim 7$ mg/mL based on $c^{**} \sim (^{10}/_3)c^*$, and the $c^{**} = 7-11$ mg/mL calculated from eq 8, are close to each other. There is a difference between the observed c^{**} value (~30 mg/mL) and these calculated c^{**} values. The reason for these discrepancies is not clear to us at this point. It is possible that such discrepancies can be reduced or even eliminated once more precise values of molecular parameters of amylose become available and are used in the c^{**} calculations, or better theoretical methods are developed to evaluate c^{**}. However, one should keep in mind that given the complexity of the concentrated regime, it is not unusual to find such differences between theory calculations and experimental observations. The observed $c^{**} \sim 30$ mg/mL is used hereafter for the discussion of results, and this choice is supported by our DLS data as discussed in the next section.

As mentioned above, at $c \ge 40$ mg/mL, the fractal plot in general gives better fits than other plotting methods. Figure 3 shows the results of the fractal plots on two sets of data at two concentrations, $c = 40.0$ and 50.0 mg/mL. These two plots give an average fractal dimension $d_f \sim 0.5$. However, it must be pointed out that in the concentrated regime $c \ge c^{**} \sim 30$ mg/mL only these two sets of data could be fit reasonably well (reduced $\chi^2 \sim 10^2$) by fractal plot. This fractal dimension interpretation should be used with caution.

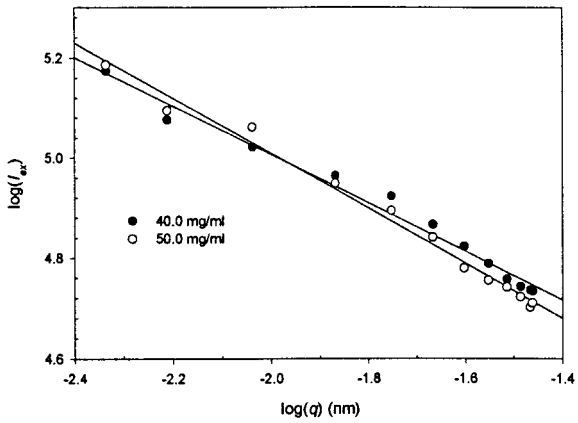

Figure 3. Fractal plots, according to eq 4, for two amylose solutions of concentrations $c = 40.0$ and 50.0 mg/mL, respectively.

It has been demonstrated that a dimensionless particle scattering factor can be defined for finite concentrations,[4]

$$P_{(q,c)} = \frac{S_{(q,c)}}{S_{(0,c)}} \tag{9}$$

where $S_{(q,c)}$ is the structure factor and $S_{(0,c)}$ is the corresponding value at scattering angle $\theta = 0$ (forward scattering). Figure 4 shows the same sets of data, as partially presented in Figure 1, normalized with forward scattering and plotted against qR_G. In the reported study,[4] all curves in the entire concentration range (1.3−12.7 mg/mL with $c^* = 2.8$ mg/mL) could be fitted into a single master curve, whereas in our case two different master curves must be used for different concentration regions. In the region with concentrations of $c < c^*$, a master curve with $R_G = 63.1$ nm (obtained via eq 6 for $c = 0$, as discussed above) is used to fit all the curves in this region, as shown in Figure 4. While in the concentration region with $c^* < c \leq c^{**}$, another master curve with a different R_G, $R_G = 40$ nm (an estimated R_G for $c \sim c^*$), is used to fit all the scattering curves in this region, as shown in Figure 5. The master curves are calculated via the following relationship,[1,4,29]

$$P_{(q)} = (1 + R_G{}^2q^2/3)^{-1} \tag{10}$$

The fact that the scattering factors of different concentrations can be fitted into a master curve indicates that the shape of the macromolecule is not changed by the thermodynamic intermolecular interactions. However, as shown by our results, different master curves must be used for different concentration regions. This does not necessarily suggest that the shape of the macromolecule is changed when the concentration is changed into another concentration region (e.g., from dilute to semidilute, etc.). More likely this is the result of the fact that in different concentration regions the macromolecular association phenomena are drastically changed, and in each concentration region, a different master curve is needed to fit the macromolecules' scattering factors. In other words, the scattering factors from different concentration regions cannot be fitted universally. As for the case of the cited literature,[4] the reported concentration range is 1.3−12.7 mg/mL, with $c^* = 2.8$ mg/mL. Therefore, it can be regarded that the whole concentration range was within the semidilute

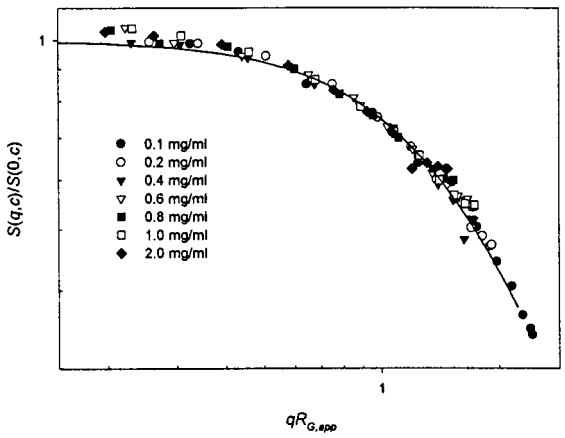

Figure 4. SLS data of different concentrations in the dilute solution regime. Data are normalized against the forward scattering, as explained in the text. The line corresponds to a master curve calculated by eq 10 using $R_G = 63.1$ nm.

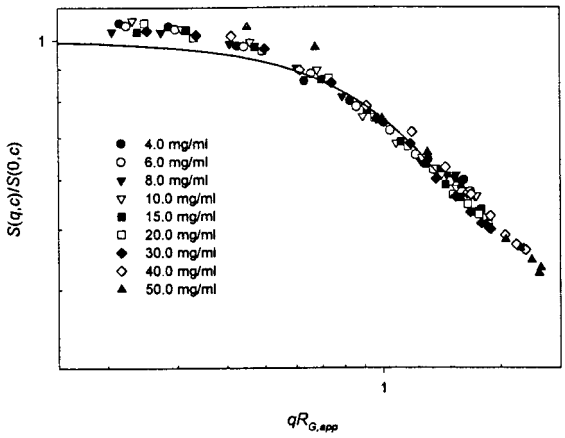

Figure 5. SLS data of different concentrations in the regions of $c > c^*$. Data are normalized against the forward scattering, as explained in the text. The line corresponds to a master curve calculated by eq 10 using $R_G = 40$ nm.

regime, and a single master curve could be used. In our case, the concentration range covers 3 orders of magnitude, and it is apparent that different master curves are needed for the dilute and the semidilute regimes. As for the concentrated region $c > c^{**}$, the data sets do not collapse into a master curve after being normalized by their respective forward scattering. The reason for this could be rather complicated: the raw data are quite scattered; the appropriateness of the fitting methods are in question. Moreover, little theoretical work has been done in this concentrated regime for us to use as guidelines, and further studies are much needed.

Dynamic Properties. Figure 6 shows the correlation functions measured by DLS at different scattering angles for amylose in DMAc−3% LiCl solution of $c = 0.4$ mg/mL. At this low concentration, the correlation functions are dominated by a single decay mode, which is presumably related to the translational diffusion motion of the amylose macromolecules. As the concentration is increased to $c \sim 6$ mg/mL, a second decay mode becomes noticeable in the correlation function, and this effect becomes more profound as the concentration increases. This is clearly demonstrated in Figure 7, which shows the correlation functions, all measured at $\theta = 90°$, of amylose solutions of five representative concentrations. The correlation functions were then analyzed by the REPES program, as discussed in the

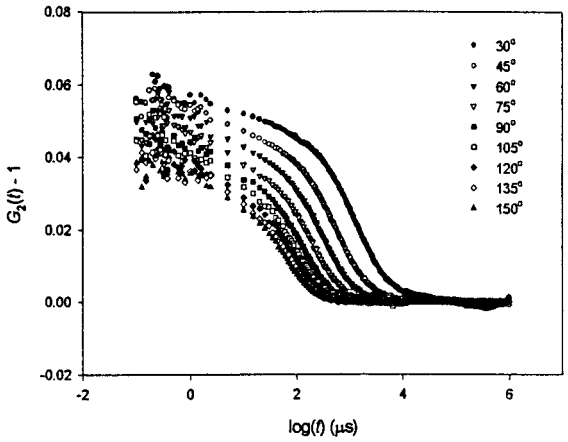

Figure 6. Intensity autocorrelation functions of amylose in DMAc−3% LiCl at different scattering angles, measured at 25.0 °C by DLS. $c = 0.4$ mg/mL.

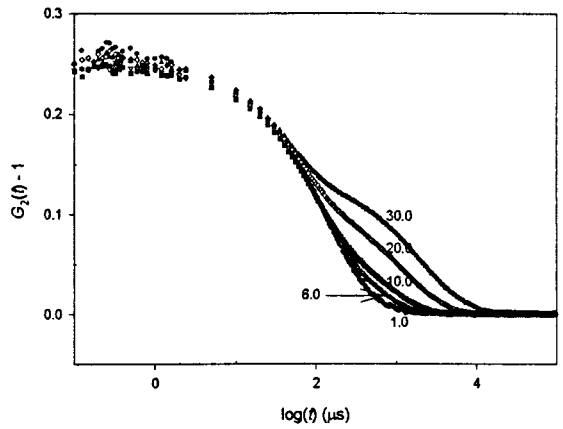

Figure 7. Intensity autocorrelation functions of amylose in DMAc−3% LiCl solutions of different concentrations, measured by DLS at 25.0 °C, scattering angle $\theta = 90°$. Notice that as concentration increases, a second decay mode becomes apparent, as compared to the low concentration where a single decay mode is present. Concentrations in milligrams per milliliter are indicated.

Experimental Section, to obtain the diffusion coefficient distribution. Figure 8 shows the distributions corresponding to the correlation functions in Figure 7 after the REPES procedure. (The REPES program has a regulator called "probability to reject" that can be used to control the appearance of the distribution peaks, to separate or to merge peaks. To be consistent, a 0.5 probability to reject was used in all of our analysis routines, and the results are reported without any further modification.)

The correlation functions can be divided into two groups, according to their appearance and to the outcome of the REPES analysis. The first group consists of the correlation functions from solutions in the concentration range $0.1 \leq c \leq 4.0$ mg/mL. All of the correlation functions in this group are dominated by one major decay process, while some of the correlation functions show a second, minor decay and the others do not. This is clearly shown as in the diffusion distribution profile obtained by REPES for 1.0 mg/mL solution, in Figure 8. The distribution is dominated by a peak at decay time $\tau \sim 3.5 \times 10^2$ μs with a minor peak at $\tau \sim 2$ μs. Not only are the appearance and the disappearance of this minor peak not consistent at different scattering angles and concentrations, but also its positions (τ values) do not have any apparent q

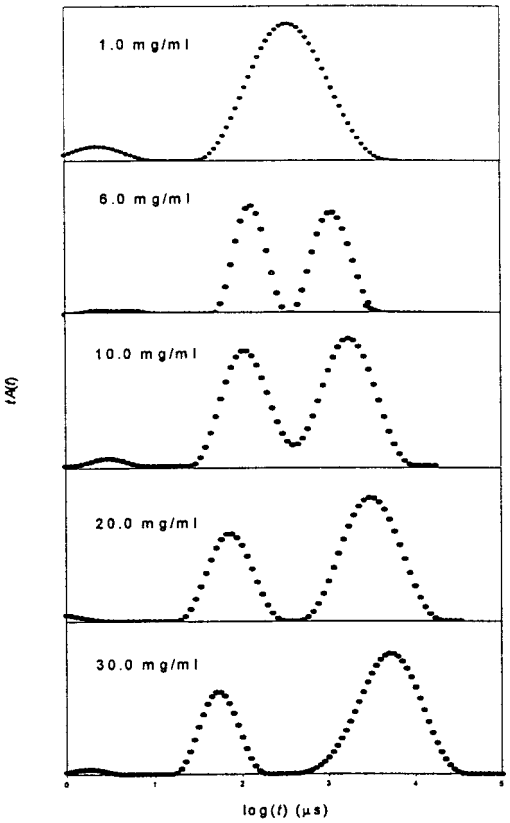

Figure 8. REPES analysis results of the intensity autocorrelation functions for amylose solutions of different concentrations, as shown in Figure 7. Note that at low concentration only a single mode is present, whereas at higher concentrations two distinguishable modes are present. The gap between the two modes (the decay time difference) widens as the concentration increases.

dependence. In other words, no physical meaning could be found for this particular peak. Therefore, this peak is regarded as instrument noise, and no further attention is paid to it in the analyses and discussions that are to follow. The dominant peak is regarded as the sole decay for the corresponding correlation functions. Given the low concentration ($c \leq 4.0$ mg/mL), it is safe to assume that this decay represents the translational diffusion motion of amylose macromolecules in dilute solution. From $c_{R_G}^* \sim 2$ mg/mL, as estimated from our SLS data, this seems to be a sound assumption. The q dependence of the decay rates of this diffusion process was then studied, and Figure 9A shows a typical set of results. The linear relationship between the decay rate Γ ($\Gamma = 1/\tau$) and q^2 proves that indeed this decay does represent the macromolecule's translational diffusion motion. The diffusion coefficient, D_m, can then be calculated via the following relationship,

$$\Gamma_m = D_m q^2 \tag{11}$$

where m denotes that the motion is due to the macromolecule's translational diffusion motion.

The second group consists of correlation functions from solutions of higher concentrations. At $c \geq 6.0$ mg/mL, it is evident that the correlation functions have more than one decay, and the REPES results (Figure 8) show that the distribution profiles are dominated by two peaks. A third, comparatively minor peak at $\tau \sim 10^0-10^1$ μs is regarded as instrument noise, for reasons as mentioned above, and no further attention is paid

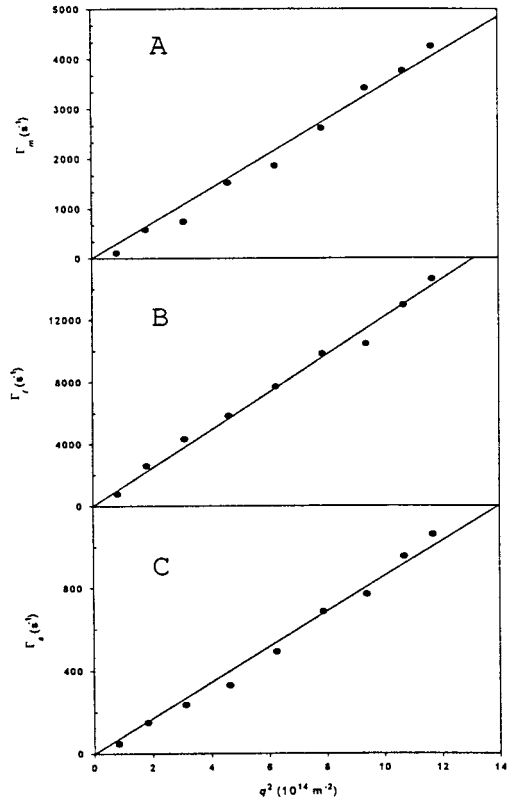

Figure 9. (A) q-Dependence of the decay rate Γ_m, as obtained by the REPES analysis, for $c = 1.0$ mg/mL of amylose solution. The line represents a linear least-squares fit, and the slope gives the diffusion coefficient $D_m = (3.81 \pm 0.13) \times 10^{-8}$ cm^2/s. The standard deviation shows the uncertainty of the fit. (B) q-Dependence of the decay rate Γ_f, for $c = 10.0$ mg/mL. $D_f = (1.19 \pm 0.047) \times 10^{-7}$ cm^2/s. (C) q-Dependence of the decay rate Γ_s, for $c = 10.0$ mg/mL. $D_s = (9.18 \pm 0.32) \times 10^{-9}$ cm^2/s. Note that $D_f > D_m > D_s$.

to it. The two dominant peaks represent two different motions in these amylose solutions. These two motions are assigned as the fast mode with the decay rate Γ_f, and the slow mode with the decay rate Γ_s. The linear q^2 dependence of Γ_f and Γ_s, as shown in parts B and C, respectively, of Figure 9 demonstrates that both motions are diffusional. By using eq 11, two diffusion coefficients D_f and D_s, corresponding to the fast and the slow diffusion modes, are then obtained from Γ_f and Γ_s, respectively.

Figure 10 summarizes the results of D_m, D_f, and D_s. At $c \leq 4.0$ mg/mL, translational diffusion of amylose macromolecules dominates the dynamic properties of the solution. A linear least-squares fit of D_m versus c shows the following relationship: D_m (cm^2/s) $= (4.28 \pm 0.30) \times 10^{-8} + (1.18 \pm 3.25) \times 10^{-9}\, c$ (c is in mg/mL). This linear relationship between D_m and c is generally expected for polymers in dilute solutions,[13,16,30]

$$D_{(c)} = D_0(1 + k_d c) \tag{12}$$

where k_d is the diffusion second virial coefficient. However, our D_m values in this region are quite scattered, which is reflected by the large uncertainty of the slope of the fitting. The intercept, $D_{m(c=0)} = (4.28 \pm 0.30) \times 10^{-8}$ cm^2/s, can be regarded as the amylose macromolecule's translational diffusion coefficient without any intermolecular interactions and therefore can be used to calculate the hydrodynamic radius R_H via the Stokes–Einstein equation,[16]

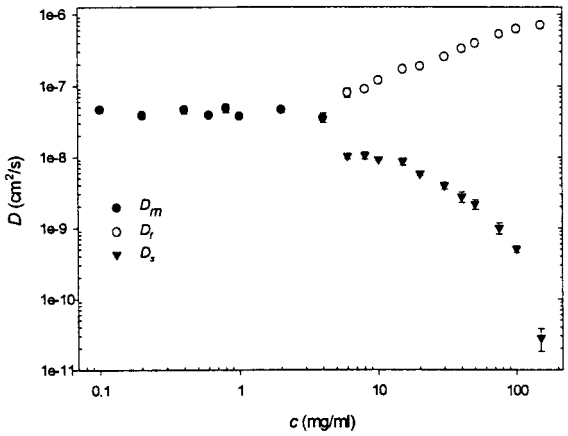

Figure 10. Concentration dependence of D_m, D_f, and D_s for amylose solution. At $c \leq 4.0$ mg/mL, only D_m is present, whereas at $c \geq 6.0$ mg/mL, D_f and D_s are present.

$$R_H = \frac{k_B T}{6\pi\eta D} \tag{13}$$

An $R_H = 37.6$ nm is obtained by using $\eta = 1.354$ cP[13] and $D_{m(c=0)} = (4.28 \pm 0.30) \times 10^{-8}$ cm^2/s. Correspondingly, the ρ parameter

$$\rho = R_G/R_H \tag{14}$$

is calculated to be $\rho_{(c=0)} = 1.68$ ($R_G = 63.1$ nm, and $R_H = 37.6$ nm). The ρ parameter has been calculated for different chain conformations, architectures, and polydispersity,[31] and $\rho \sim 1.7$ indicates a system of polydisperse random coils in Θ solvent. At first glance, this was surprising, since other solvent systems such as aqueous KOH and DMSO/H_2O have been identified as good solvents for amylose. The value of k_d, the diffusion second virial coefficient, will shed some light on this. From eq 12, k_d is estimated to be (27.5 ± 75.9) mL/g. (The large uncertainty indicates that the data were rather scattered.) By using the relationship $k_d \approx 2A_2M_W$, and $M_W \sim 10^6$ g/mol, $A_2 \sim 10^{-5}$ mol mL/g^2 was then obtained. This A_2 value close to 0 then indicates that indeed this is a system close to Θ conditions.

As the concentration increases, the dynamics of the solution undergo a transition. This transition occurs at $c = 4-6$ mg/mL, as shown in Figure 10: at $c \leq 4$ mg/mL, a single diffusion mode (D_m) is present in the solution, whereas at $c \geq 6$ mg/mL, two independent diffusion modes (D_f and D_s) are present. This transition can be understood as the transition from dilute solution regime to semidilute solution regime. This point is illustrated as follows. The value for the overlap concentration c^* can also be theoretically calculated, according to the following relationship,[21]

$$c_{R_H}{}^* = \frac{M_W/N_A}{4\pi/3R_H^3} \tag{15}$$

By use of $R_H = 37.6$ nm, combined with the same M_W values as used in calculating $c_{R_G}{}^*$, eq 15 gives $c_{R_H}{}^*$ in the range of 3.7−15 mg/mL. The observed transition concentration, i.e., $c = 4-6$ mg/mL, falls into the calculated $c_{R_H}{}^*$ range, indicating that this is indeed the dilute to semidilute transition. Furthermore, these $c_{R_H}{}^*$ values, both calculated ($c_{R_H}{}^* = 3.7-15$ mg/mL) and observed ($c_{R_H}{}^* = 4-6$ mg/mL), also are in agreement with the $c_{R_G}{}^*$ values, i.e., $c_{R_G}{}^* = 0.8-3$ mg/mL (calcu-

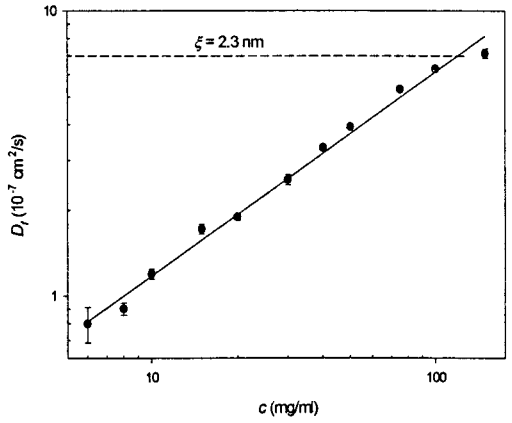

Figure 11. The log−log plot of D_f versus c. The solid line represents a linear least-squares fit with a slope of 0.72 ± 0.02. The linear relationship between log(D_f) versus log(c) corresponds to $D_f \sim c^{(0.72 \pm 0.02)}$. This compares well with de Gennes' scaling relation $D_f \sim c^{3/4}$. The dashed line shows that at the highest concentration the network has a correlation length of $\xi = 2.3$ nm.

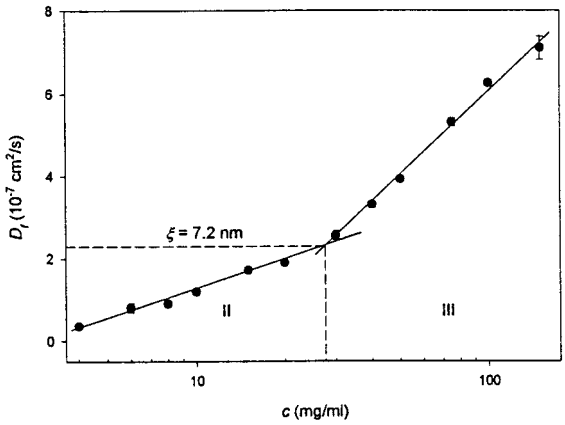

Figure 12. The same data set as in Figure 11, but now plotted on this semilog plot as D_f versus log(c). Two distinguishable regions are apparent, designated as II and III (in corresponding to the nomenclature in Figure 2). D_f has a stronger c dependence in region III than that in region II; in region II, $D_f \sim (2.44 \pm 0.15)\log(c)$; in region III, $D_f \sim (6.78 \pm 0.25)\log(c)$. The solid lines are linear least-squares fits for the two regions, respectively. The transition from II to III occurs at $c \sim 30$ mg/mL. The dashed line corresponds to the correlation length of $\xi = 7.2$ nm of the network when the transition occurs.

lated) and $c_{R_G}^* \sim 2$ mg/mL (observed). (By definition, $c_{R_H}^*$ and $c_{R_G}^*$ differ by a factor of ρ^3, where $\rho = R_G/R_H \sim 1.7$.)

Figure 10 shows that in the $c \geq 6.0$ mg/mL region two diffusion modes are present: D_f and D_s. For the interpretation of solution dynamics at concentration $c \geq c^*$, a scaling approach was proposed by de Gennes.[32] According to the scaling model, linear chains in the $c \geq c^*$ regime overlap to form a transient interpenetrating network. The scaling theory predicts two types of motion for linear chains in $c \geq c^*$ regime: (1) a fast diffusion D_f (cooperative diffusion D_{coop}), which is a measure of the network's correlation length ξ via the Stokes−Einstein type of equation ($\xi = k_B T/6\pi\eta D_f$), and (2) a slower one D_s (reptation diffusion D_{rep}), which originates from chain reptation, i.e., the motion of individual chains along their contour length through the entangled network. (This motion resembles the movement of the snake, hence the name reptation.) For linear chains in a good solvent, de Gennes predicts the following scaling relationships

$$D_f \sim c^{3/4} \tag{16}$$

$$D_s \sim c^{-7/4} \tag{17}$$

For linear chains in Θ solvent, the theory predicts a concentration dependence for D_f with an exponent of 1 and for D_s with an exponent of −3.

As shown in Figure 10, D_f increases as concentration increases, while D_s decreases as concentration increases. Therefore, qualitatively, they fit into de Gennes' description of cooperative diffusion and reptation diffusion, respectively. Figure 11 shows the log−log plot of D_f versus c, with a slope of 0.72. The scaling relationship $D_f \sim c^{0.72}$ is thus obtained. According to de Gennes' scaling theory, such a scaling relationship indicates linear chains in good solvent. However, our calculated ρ value ($\rho \sim 1.7$) and the derived A_2 value (from the diffusion second virial coefficient k_d) suggest that this is a system close to Θ conditions. The reason for this discrepancy is not clear to us at this point, and more work is certainly needed. As shown in Figure 11, the D_f for the highest concentration corresponds to a correlation length $\xi = 2.3$ nm. (ξ can often be viewed as the mesh size of the network.) However, unlike other published work on starch, where an upper D_f limit was reported at c $\sim$ 100 mg/mL,[3] no such limit was seen in our study for concentration as high as 150 mg/mL.

The $D_f \sim c^{0.72}$ scaling relationship seems to fit into de Gennes' scaling model, at least qualitatively. However, when a D_f versus log(c) plot is used, a totally different picture is obtained, as shown in Figure 12. The D_f versus c scaling relation undergoes a transition at $c \sim 30$ mg/mL: at $c \leq 30$ mg/mL, D_f versus c scales as $D_f \sim (2.44 \pm 0.15)\log(c)$, whereas at c $\geq$ 30 mg/mL, D_f versus c scales as $D_f \sim (6.78 \pm 0.25)\log(c)$. In other words, D_f has a much stronger dependence on c at $c \geq$ 30 mg/mL than at $c \leq 30$ mg/mL. This transition occurs at c $\sim$ 30 mg/mL where $D_f = 2.22 \times 10^{-7}$ cm^2/s, which corresponds to a correlation length $\xi = 7.2$ nm. The significance of this ξ value, at which this transition occurs, is not clear to us at this point.

According to our SLS results, the transition from semidilute regime to concentrated regime occurs at $c^{**} \sim 30$ mg/mL. Therefore, the above results can be interpreted as indicating that D_f has stronger c dependence in the concentrated regime than in the semidilute regime. This phenomenon can be understood as the following. In the semidilute regime, macromolecules start to overlap to form aggregates (or clusters) and regional networks. However, there is also a void volume (pure solvent regions) present in the semidilute solution regime; i.e., the clusters (or regional networks) are separate identities, separated by pure solvent regions. As the concentration increases, part of the added macromolecule mass goes to increase the cluster's size and density, reducing the correlation length ξ and thus increasing D_f; the rest of the added macromolecule mass goes to fill the void volume. In other words, in the semidilute regime, only part of the added macromolecule mass contributes to increase D_f. On the other hand, in the concentrated regime, the solvent molecules are distributed rather uniformly throughout the system, and the whole solution can be regarded as a homogeneous medium. As the concentration increases, all of the added macromolecule mass goes to increase the density of the entangled network, reducing the correlation

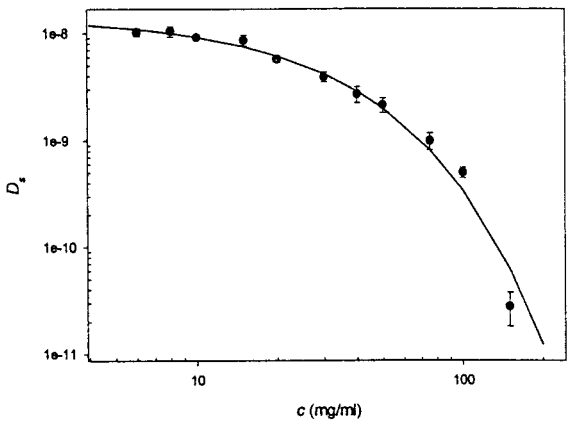

Figure 13. Concentration dependence of the slow mode D_s. The solid line corresponds to a fit according to eq 18 with an exponent of $\mu = 0.918 \pm 0.039$. The standard deviation shows the uncertainty of the fit.

length ξ and thus increasing D_f. In summary, D_f has a stronger c dependence in the concentrated regime because all the added c goes to increase D_f, as compared to the semidilute regime where only part of the added mass works to increase D_f while the rest of the added mass goes to fill the void volume.

That the c dependence of D_f undergoes a transition from the semidilute regime to the concentrated regime is contrary to de Gennes' theory that one scaling relationship (eq 16) applies to both of these regimes. However, to our knowledge, this is the first time that such phenomenon has been reported, whereas there are ample reports supporting de Gennes' scaling relationship (eq 16). We are not certain whether our finding only applies to this particular corn amylose/DMAc−3% LiCl system, or if it applies to polymer systems in general. More studies are certainly needed. One thing is worth noting. Equation 16 is often reported when using log(D_f) versus log(c) plots. However, log−log plots are notorious for yielding seemingly straight lines. This is clearly demonstrated in our case: when the log(D_f) versus log(c) plot is used, a straight line is obtained with an exponent close to that of de Gennes' prediction, as shown in Figure 11. When the more sensitive semilog plot, D_f versus log(c) plot, is used, a totally different picture is obtained, as shown in Figure 12.

The monotonic decrease of D_s as concentration increases, as shown in Figure 10, can be best described by a "stretched exponential decay" fitting, as shown in Figure 13. This is apparently not the chain reptation motion. The theory that fits our data pattern the best is this "stretched exponential" scaling relation for a diffusion probe's motion in a polymer matrix.

$$D_s = D_0 \exp(-\alpha c^{\mu}) \tag{18}$$

The exponent $\mu \sim 0.6-1$ has been reported for hard spheres as a probe and flexible coils as the matrix polymer.[33−38] The fitting of our D_s versus c data, according to eq 18, gives $D_0 = (1.45 \pm 0.15) \times 10^{-8}$ cm^2/s, $\alpha = -(0.0546 \pm 0.0074)$, and $\mu = (0.918 \pm 0.039)$. This μ value compares well with reported values for tracer diffusion probes in a polymer matrix. The $D_0 = (1.45 \pm 0.15) \times 10^{-8}$ cm^2/s is much smaller than the diffusion coefficient for the amylose macromolecule, $D_{m(c=0)} = (4.28 \pm 0.30) \times 10^{-8}$ cm^2/s; i.e., the dimensions of the particles responsible for D_s are much bigger ($R_H \geq 110$ nm) than that of the amylose macromolecule. The D_s versus c relationship does not follow the prediction by de Gennes' reptation model. Instead, it fits the description of the probe diffusion in a polymer matrix; it is therefore concluded that D_s does not represent reptation diffusion motion but may reflect the motion of aggregate/cluster diffusion. However, it is hard to picture how these extremely large clusters can pass through the transient network in the semidilute and concentrated regimes, where the correlation length for the network can be as small as only a few nanometers. A plausible explanation was proposed by Galinsky and Burchard,[3] that the motion of the center of the mass results from the random forming and breaking of bonds, which would indeed result in an apparent motion of the clusters. In other words, the aggregates/clusters are temporal: they are constantly in the state of breaking and reforming. This view is supported by the fact that such slow motions completely disappear if the networks are formed by covalent bonds. Moreover, in our view, the transient network could break and reform as well, thus assisting these temporal clusters' motion through the network. Such temporal clusters have also been reported by Sedlak to be responsible for the slow diffusive mode in polyelectrolyte systems.[39]

The fact that no reptation-like motion has been observed can be explained as follows. The scattering signal from chain reptation motion is much weaker than that from cluster diffusion motion, since the clusters are much larger in size. Moreover, because the relaxation times of these two motions are close to each other, it is likely that these two peaks overlap. Therefore, in the REPES analysis, the reptation motion peak is probably buried in the slow cluster motion peak, D_s. Since the reptation motion is rather weak, its contribution to the REPES analysis results is probably negligible. We do not expect the REPES results, D_s values in particular, to be greatly influenced by it.

Another feature of the REPES analysis is that it gives the relative amount of each diffusion mode, A_i, i = f for the fast mode and i = s for the slow mode. By analyzing the q dependence for the relative amount of A_s/A_f for concentration range $c = 6.0-150$ mg/mL, it is apparent that A_s/A_f has a linear relationship with q^2,

$$A_s/A_f = (A_s/A_f)_{(q=0)} - aq^2 \tag{19}$$

where $(A_s/A_f)_{(q=0)}$ is the intercept at $q^2 = 0$ and a is a constant. The increasing of A_s/A_f as q^2 decreases probably results from the stronger angular dependence of the large particles' scattering functions. Figure 14 shows a typical plot of A_s/A_f versus q^2, and $(A_s/A_f)_{(q=0)}$ and a are obtained by linear least-squares fit. Figure 15 summarizes the concentration dependence for $(A_s/A_f)_{(q=0)}$ at different concentrations. It is apparent that $(A_s/A_f)_{(q=0)}$ increases as c increases, indicating that as concentration increases the amount of clusters increases, as one should expect. Moreover, the following relationship is found for $(A_s/A_f)_{(q=0)}$ and c,

$$(A_s/A_f)_{(q=0)} = -(1.93 \pm 1.33) + (4.12 \pm 0.88) \log(c) \tag{20}$$

Figure 16 shows the concentration dependence of the constant a, as obtained from eq 19 for each of the individual concentrations. A linear least-squares fit of

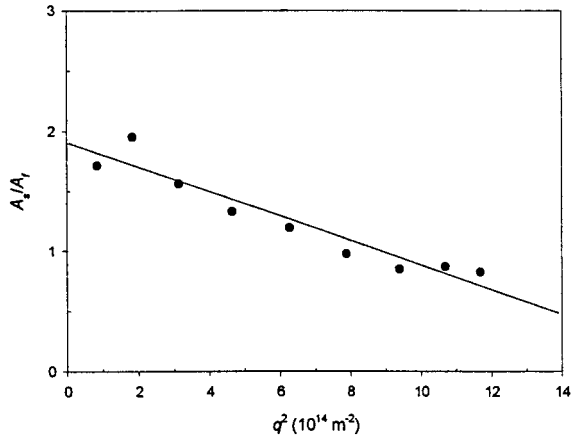

Figure 14. Relative amounts of the slow mode and the fast mode plotted as a function of q^2. The line corresponds to a linear least-squares fit according to eq 19. The intercept at $q = 0$ give A_s/A_f at scattering angle $\theta = 0°$, i.e., $(A_s/A_f)_{(q=0)}$. The slope gives the constant a.

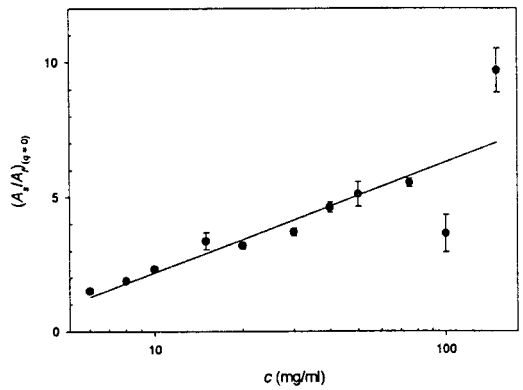

Figure 15. Concentration dependence of $(A_s/A_f)_{(q=0)}$. The solid line corresponds to a linear least-squares fit of $(A_s/A_f)_{(q=0)}$ versus log(c), which gives $(A_s/A_f)_{(q=0)} \sim (4.12 \pm 0.88)\log(c)$. The increasing $(A_s/A_f)_{(q=0)}$ as concentration increases shows that the relative amount of clusters increases with concentration. $(A_s/A_f)_{(q=0)}$ Values for each concentration are determined by eq 19, as shown in Figure 14.

a versus c gives the following relationship,

$$a = -(9.48 \pm 4.26) \times 10^{-2} + (3.16 \pm 0.67) \times 10^{-3} \log(c) \quad (21)$$

Equation 19 shows the principle that larger particles have stronger angular dependence, and in general, eqs 20 and 21 show that as concentration increases, the amount of large particles (clusters) increases, thus the increased angular dependence. However, since there is no theoretical work in this area that we can use as a guide, the exact physical meanings of these linear relationships shown as eqs 19−21 are not clear to us at this point.

It is also a common practice to analyze the correlation functions for stretched exponential decays and power-law decays.[40] No such relationships have been found on a consistent basis for our correlation functions throughout the whole concentration range. It is often stated, that in order to have such decay behaviors, the polymers need to be branched so that the interpenetrating clusters and networks can be formed. The lack of such stretched exponential decays and power-law decays in our system is another indication that corn amylose macromolecules are by and large linear macromolecules.

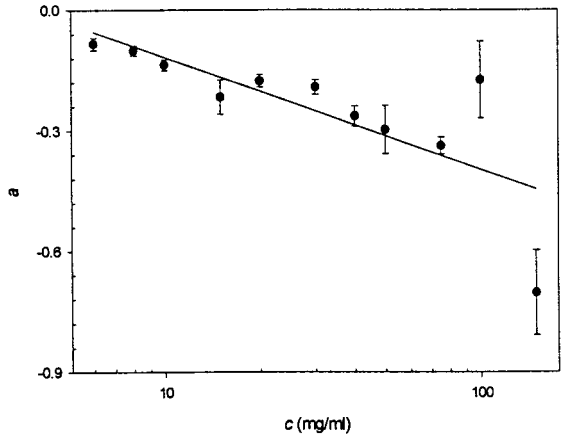

Figure 16. The concentration dependence of a, the constant in eq 19. The solid line corresponds to a linear least-squares fit of a versus log(c), which gives $a \sim (3.16 \pm 0.67) \times 10^{-3}$ log(c). The decreasing a as concentration increases shows the increasing angular dependence of the clusters (probably related to the increasing dimension) with concentration. Values of a for each concentration are determined by eq 19, as shown in Figure 14.

Conclusion

The static solution properties of corn amylose in DMAc−3% LiCl can be divided into three regions, identified as the dilute, the semidilute, and the concentrated solution regimes, respectively. The values of c^* and c^{**} were evaluated. The observed c^* and c^{**} values, both from static data and dynamic data, agree well with each other and with the calculated values. The dimensions of amylose macromolecules and clusters in these regimes are evaluated by appropriate methods. DLS data show that at $c < c^*$, one diffusion motion D_m, which represents the amylose macromolecule's translational diffusion, is present in the solution. At $c > c^*$, two distinguishable diffusion modes are present, D_f and D_s. D_s's concentration-dependence pattern suggests that it represents the translational diffusion motion of amylose clusters. Further analysis shows for the first time that D_f has two distinguishable concentration dependence patterns at $c^* < c < c^{**}$ and at $c > c^{**}$, in contrast to a uniform D_f versus c relationship for $c > c^*$ regions as proposed by de Gennes. This change in D_f can be used as an indicator of the transition from semidilute regime to the concentrated regime. The relative amounts of these two modes are analyzed, and their relationships with the concentration are presented.

Acknowledgment. Comments on the manuscript by Dr. C. J. Carriere of NCAUR are gratefully acknowledged. This research was conducted under CRADA Number 58-3K95-8-0632 between Agricultural Research Service and Biotechnology Research and Development Corporation.

References and Notes

(1) Aberle, T.; Burchard, W.; Galinsky, G.; Hanselmann, R.; Klingler, R. W.; Michel, E. *Macromol. Symp.* **1997**, *120*, 47−63.
(2) Aberle, T.; Burchard, W. *Starch* **1997**, *49*, 215−224.
(3) Galinsky, G.; Burchard, W. *Macromolecules* **1996**, *29*, 1498−1506.
(4) Galinsky, G.; Burchard, W. *Macromolecules* **1997**, *30*, 4445−4453.
(5) Galinsky, G.; Burchard, W. *Macromolecules* **1995**, *28*, 2363−2370.

(6) Galinsky, G.; Burchard, W. *Macromolecules* **1997**, *30*, 6966−6973.
(7) I'Anson, K.; Morris, V. J.; Ring, S. G. *Prog. Biotechnol.* **1985**, *1*, 115−119.
(8) Ring, S. G.; I'Anson, K. J.; Morris, V. J. *Macromolecules* **1985**, *18*, 182−188.
(9) Roger, P.; Tran, V.; Lesec, J.; Colonna, P. *J. Cereal Sci.* **1996**, *24*, 247−262.
(10) Roger, P.; Colonna, P. *Int. J. Bio. Macromol.* **1996**, *19*, 51−61.
(11) Roger, P.; Colonna, P. Use of Light Scattering to Characterize the Polysaccharides of Starch. *NATO ASI Ser.*, 3 1997. *Light Scattering and Photon Correlation Spectroscopy Ser. 3*. Pike, E. R., Abbiss, J. B., Eds.; **1997**, 225−229.
(12) Dawsey, T. R.; McCormick, C. L. *J.M.S.- Rev. Macromol. Chem. Phys.* **1990**, *C30*, 405−440.
(13) Ying, Q.; Chu, B. *Macromolecules* **1987**, *20*, 871−877.
(14) Schoch, T. J. *J. Am. Chem. Soc.* **1942**, *64*, 2957−2961.
(15) Knutson, C. A. *Carbohydr. Polym.*, accepted for publication.
(16) Cao, X.; Sessa, D. J.; Wolf, W. J.; Willett, J. L. *J. Appl. Polym. Sci.*, submitted for publication.
(17) Jakes, J. *Collect. Czech. Chem. Commun.* **1995**, *60* (11), 1781−1797.
(18) Jakes, J. *Czech. J. Phys.* **1988**, *38*, 1305−1316.
(19) Johnsen, R. M.; Brown, W. In *Laser Light Scattering in Biochemistry*; Harding, S. E., Sattelle, D. B., Bloomfield, V. A., Eds.; The Royal Society of Chemistry: Cambridge, 1992; pp 77−91.
(20) Stepanek, P.; Johnsen, R. M. *Collect. Czech. Chem. Commun.* **1995**, *60*, 1941−1949.
(21) Freed, K. F. *Renormalization Group Theory of Macromolecules*; Wiley: New York, 1987.
(22) Roger, P.; Bello-Perez, L. A.; Colonna, P. *Polymer* **1999**, *40*, 6897−6909.
(23) Ferry, J. D. *Viscoelastic Properties of Polymers*; John Wiley & Sons: New York, 1980.
(24) Doi, M.; Edwards, S. F. *The Theory of Polymer Dynamics*; Oxford Press: London, 1988.
(25) Macosko, C. W. *Rheology*: *Principles, Measurement, and Applications*; VCH Publications: New York, 1994.
(26) Carriere, C. J. *J. Polym. Sci., Part B*: *Polym. Phys.* **1998**, *36*, 2085−2093.
(27) Hanemann, O.; Ballauff, M. *Macromolecules* **1997**, *30*, 7638−7640.
(28) Momany, F., personal communication.
(29) Burchard, W. *Macromolecules* **1977**, *10*, 919−927.
(30) Yamakawa, H. *Modern Theory of Polymer Solution*; Harper and Row: New York, 1971.
(31) Burchard, W.; Schmidt, M.; Stockmayer, W. H. *Macromolecules* **1980**, *13*, 1265−1272.
(32) de Gennes, P. G. *Scaling Concepts in Polymer Physics*; Cornell University Press: Ithaca and London, 1979.
(33) Cao, X.; Bansil, R.; Gantz, D.; Moore, E. W.; Niu, N.; Afdhal, N. H. *Biophys. J.* **1997**, *73*, 1932−1939.
(34) Pu, Z.; Brown, W. *Macromolecules* **1989**, *22*, 890−896.
(35) Phillips, G. O.; Peczak, P. *Macromolecules* **1988**, *21*, 214−220.
(36) Phillips, G. O. *Macromolecules* **1988**, *21*, 3101−3106.
(37) Phillips, G. O. *Macromolecules* **1990**, *23*, 2742−2748.
(38) Brown, W.; Rymden, R. *Macromolecules* **1988**, *21*, 840−846.
(39) Sedlak, M. *J. Chem. Phys.* **1996**, *105*, 10123−10133.
(40) Cao, X.; Bansil, R.; Bhaskar, R.; Turner, B. S.; LaMont, J. T.; Niu, N.; Afdhal, N. H. *Biophys. J.* **1999**, *76*, 1250−1258.

MA9918248